




Low-dissipation engines: Microscopic construction via shortcuts to adiabaticity and isothermality, the optimal relation between power and efficiency

Xiu-Hua Zhao ¹, Zheng-Nan Gong,² and Z. C. Tu ^{1,*}

¹*Department of Physics, Beijing Normal University, Beijing 100875, China*

²*Zun Yi Si Zhong, Zunyi 563000, China*

 (Received 18 June 2022; revised 13 October 2022; accepted 27 November 2022; published 15 December 2022)

We construct a microscopic model of low-dissipation engines by driving a Brownian particle in a time-dependent harmonic potential. Shortcuts to adiabaticity and shortcuts to isothermality are introduced to realize the adiabatic and isothermal branches in a thermodynamic cycle, respectively. We derive an analytical formula of the efficiency at maximum power with explicit expressions of dissipation coefficients under the optimized protocols. When the relative temperature difference between the two baths in the cycle is insignificant, this expression satisfies the universal law of efficiency at maximum power up to the quadratic term of the Carnot efficiency. For large relative temperature differences, the efficiency at maximum power tends to be $1/2$. Furthermore, we analyze the issue of power at any given efficiency for general low-dissipation engines and then obtain the supremum of the power in three limiting cases, respectively. These expressions of maximum power at given efficiency provide the optimal relations between power and efficiency which are tighter than the results in previous references.

DOI: [10.1103/PhysRevE.106.064117](https://doi.org/10.1103/PhysRevE.106.064117)

I. INTRODUCTION

Finite-time thermodynamics [1,2] is a new active branch of nonequilibrium physics. One of the most important topics in finite-time thermodynamics is the efficiency at maximum power for heat engines. Researchers have investigated the efficiencies at maximum power for various models of finite-time heat engines, including the endoreversible Carnot-like engine [3,4], stochastic engine [5], Feynman's ratchet [6], quantum dot engine [7], low-dissipation engine [8], minimally nonlinear irreversible engine [9], and so on. Their studies reveal an impressive universality that under certain conditions the efficiencies at maximum power for different models are identical up to the quadratic term of Carnot efficiency [3–7], i.e.,

$$\eta_{P_{\max}} = \frac{\eta_C}{2} + \frac{\eta_C^2}{8} + \dots, \quad (1)$$

where $\eta_{P_{\max}}$ is the efficiency at maximum power and η_C is the Carnot efficiency. It is found that the universality up to the linear term is due to the tight coupling [10] and that the universality up to the quadratic term owes to symmetric coupling [11] or energy matching [12,13].

To seek both powerful and efficient engines for practical applications, an increasing number of researchers have been devoting themselves to studying the general constraints for efficiency and power [4,8,9,14–27]. For endoreversible engines, Chen and Yan derived an optimum relation between power and efficiency [4] while Gordon and Huleihil provided the power-versus-efficiency diagram [14]. More recently,

Esposito *et al.* derived the upper and lower bounds of efficiency at maximum power for low-dissipation engines [8]. Holubec and Ryabov [18,19] discussed the efficiency at arbitrary power for low-dissipation engines and analytically obtained the maximum efficiency in the regions nearby the maximum power and the zero power. Ma *et al.* analytically derived the constraints on efficiency for all power values [24]. But their results are not the supremum or infimum in the whole region since these constraints are not always accessible. Abiuso and Perarnau-Llobet obtained the exact maximum power at any efficiency for symmetric low-dissipation engines and further optimized the overall figure of merit [25].

With the fast development of the optical-trap technique, the design and realization of microscopic engines have been widely discussed [28–34]. Schmiedl and Seifert constructed a stochastic Carnot-like engine by using a time-dependent potential to drive a Brownian particle [5]. The protocol during the isothermal process is chosen to yield a maximum work output while the adiabatic transitions are completed instantaneously. Considering that the mismatch of kinetic energy in the instantaneously adiabatic transition inevitably results in heat exchange between two heat baths, the last author in the present work proposed replacing the instantaneously adiabatic transitions with shortcuts to adiabaticity [29]. Plate *et al.* [34] constructed an overdamped Carnot-like engine with the same isothermal process while the adiabatic process is defined as no heat exchange after ensemble averaging. However, the isothermal transitions in these models are not really isothermal in the traditional sense since the effective temperature is time-dependent. This shortage inspires the subsequent researches. Following the work by Salazar and Lira [35], Chen *et al.* realized the isothermal process with exponential protocols under the assumption of slow driving

*tuzc@bnu.edu.cn

[36]. Nakamura *et al.* developed the fast-forward approach to mimic the finite-time isothermal process [37]. Their approach consists of two steps: determining the driving potential in an extremely slow time evolution and then rescaling the time variable so that the Kramers equation works for finite-time regions. A more straightforward approach is the shortcut to isothermality [38,39] which is the correspondence of quasistatic isothermal process in finite-time thermodynamics. The calculations of work and heat are tractable in shortcuts to isothermality. There is still a blank in the study of heat engines with the consideration of shortcuts to isothermality.

In this work, we employ both shortcuts to isothermality [38] and shortcuts to adiabaticity [40,41] to accomplish a microscopic finite-time Carnot-like engine. This engine turns out to be of low dissipation. We also investigate the power and efficiency of this low-dissipation engine. The rest of this paper is organized as follows. In Sec. II, we revisit the shortcuts to isothermality and shortcuts to adiabaticity. In Sec. III, we construct a microscopic heat engine including two isothermal branches and two adiabatic branches. The work dissipated during the isothermal branches is inversely proportional to the operation time, which means what we construct is exactly a model of low-dissipation engines. In Sec. IV, we calculate the efficiency at maximum power of this engine and respectively analyze its behavior at small and large relative temperature differences. We also calculate the efficiency at maximum power in the highly underdamped and overdamped limits. In Sec. V, we discuss the power at any given efficiency for general low-dissipation engines and obtain the analytical supremum of power when the ratio of dissipation coefficients during the cold and hot isothermal branches approaches zero, one and infinity, respectively. In Sec. VI, we compare our results for the bounds of efficiency at given power with those in Refs. [19,24]. The last section is a brief summary.

II. REVISITING SHORTCUTS TO ISOTHERMILITY AND SHORTCUTS TO ADIABATICITY

In this section, we outline two key concepts that we will adopt in this work. The first one is the shortcut to isothermality and the second one is the shortcut to adiabaticity.

A. Shortcuts to isothermality

Consider a Brownian particle moving in a one-dimensional potential $U_o(x, \lambda)$, where $\lambda = \lambda(t)$ is a time-dependent external parameter. The Hamiltonian of this particle is $H_o = p^2/2 + U_o(x, \lambda)$, where p is the momentum of the particle. The mass of the particle is set to be unit for convenience. The Brownian particle is coupled to a heat bath with a constant temperature T . To realize finite-time isothermal transitions between two equilibrium states with the same temperature, Li *et al.* [38,39] proposed a framework of shortcuts to isothermality by introducing an auxiliary potential $U_a(x, p, t)$ so that the distribution function of the system always maintains the following canonical form

$$\rho = e^{\beta F(\lambda) - \beta H_o(x, p, \lambda)}, \quad (2)$$

where $F = -\beta^{-1} \ln[\int \int dx dp e^{-\beta H_o(x, p, \lambda)}]$ is the Helmholtz free energy and $\beta = 1/T$. We have set the Boltzmann

constant to be unit. The auxiliary potential can be determined by substituting Eq. (2) into the generalized Kramers equation (see Eq. (19) in Ref. [38])

$$\begin{aligned} \frac{\partial \rho}{\partial t} = & -\frac{\partial}{\partial x}(p\rho) + \frac{\partial}{\partial p}\left(\gamma p\rho + \rho \frac{\partial U_o}{\partial x}\right) + \frac{\gamma}{\beta} \frac{\partial^2 \rho}{\partial p^2} \\ & - \frac{\partial U_a}{\partial p} \frac{\partial \rho}{\partial x} + \frac{\partial U_a}{\partial x} \frac{\partial \rho}{\partial p} + \gamma \frac{\partial}{\partial p}\left(\rho \frac{\partial U_a}{\partial p}\right), \end{aligned} \quad (3)$$

where γ is the damping coefficient. We assume that the original potential $U_o(x, \lambda)$ and its partial derivatives with respect to x and λ are all continuous so that the differential equation for $U_a(x, p, t)$ does not contain singular points. As for the time-dependent harmonic potential $U_o = \lambda^2(t)x^2/2$, the auxiliary potential is

$$U_a = \frac{\dot{\lambda}(t)}{2\gamma\lambda(t)}[(p - \gamma x)^2 + \lambda^2(t)x^2], \quad (4)$$

where the dot above a character denotes the derivative with respect to time t . The total Hamiltonian of the particle is $H = H_o + U_a$. To ensure that the initial and final states of the system are in equilibrium with the bath, a constraint

$$\dot{\lambda}(t_i) = \dot{\lambda}(t_f) = 0 \quad (5)$$

should be imposed at the initial time t_i and the final time t_f [38].

According to stochastic thermodynamics [42–44], the ensemble-averaged work exerted on the particle during the shortcut to isothermality is

$$\begin{aligned} W = & \left\langle \int_{t_i}^{t_f} dt \frac{\partial H}{\partial t} \right\rangle \\ = & \int_{t_i}^{t_f} dt \iint dx dp \rho \left(\frac{\partial U_o}{\partial t} + \frac{\partial U_a}{\partial t} \right) \\ = & T \ln \frac{\lambda(t_f)}{\lambda(t_i)} + T \frac{C[\Lambda]}{t_f - t_i}, \end{aligned} \quad (6)$$

where

$$C[\Lambda] = \int_0^1 d\tilde{t} \left(\frac{1}{\gamma} + \frac{\gamma}{\Lambda^2} \right) \frac{1}{\Lambda^2} \left(\frac{d\Lambda}{d\tilde{t}} \right)^2, \quad (7)$$

$\Lambda = \Lambda(\tilde{t}) = \lambda[t_i + (t_f - t_i)\tilde{t}]$, and $\tilde{t} = (t - t_i)/(t_f - t_i)$. $\langle \dots \rangle$ denotes the ensemble average under the canonical distribution (2). The work in Eq. (6) is decomposed into two parts. The first term equals the variation of the free energy. The second term represents the dissipative work which is inversely proportional to the operation time $(t_f - t_i)$. Although this result is based on the harmonic potential, the inverse-proportion relation between the dissipative work and the operation time is universal for shortcuts to isothermality [38] as long as the original potential is well-behaved, i.e., $U_o(x, \lambda)$ and its partial derivatives are continuous. This universality can be explained as follows. The auxiliary potential $U_a(x, p, t)$ can always be decomposed as $U_a(x, p, t) = \dot{\lambda}f(x, p, \lambda)$ [38]. Hence, $\partial U_a/\partial t = \dot{\lambda}f + \lambda \partial f/\partial t$. For shortcuts to isothermality, the time integral of $\langle \partial U_o/\partial t \rangle$ equals the variation of free energy of the system while the time integral of $\langle \partial U_a/\partial t \rangle$ represents the ensemble-averaged dissipative work [38,39].

Substituting $\partial U_a/\partial t = \ddot{\lambda}f + \dot{\lambda}\partial f/\partial t$ into the expression of ensemble-averaged dissipative work and replacing t with the dimensionless quantity \tilde{t} , the result is $1/(t_f - t_i)$ multiplied by an item independent of the operation time. Therefore, the dissipative work is always inversely proportional to the operation time.

B. Shortcuts to adiabaticity

Shortcuts to adiabaticity are strategies devised to circumvent the condition of infinitely slow evolution in quantum adiabatic theorem [40,45–52]. These strategies are also applicable to classical systems. In classical mechanics, the volume Ω of phase space enclosed by an energy shell remains constant when the external parameter varies slowly enough. Jarzynski introduced a counterdiabatic driving Hamiltonian H_c so that Ω will keep constant even if the external parameter changes at a finite rate [41]. As an example, Jarzynski obtained $H_c = -\dot{\lambda}(t)xp/(2\lambda(t))$ for $H_o = p^2/2 + \lambda^2(t)x^2/2$. Hence, the total Hamiltonian becomes

$$H = H_o + H_c = \frac{p^2}{2} + \frac{1}{2}\lambda^2(t)x^2 - \frac{\dot{\lambda}(t)}{2\lambda(t)}xp. \quad (8)$$

Consider the system described by the above equation decoupling from heat bath and hence the system's evolution is determined by Hamiltonian mechanics. In Ref. [29], the author found that shortcuts to adiabaticity can be adopted to ensure that the system evolves from an equilibrium state with specific temperature T_i at the initial time t_i to another equilibrium state with target temperature T_f at the final time t_f as long as the external parameter satisfies

$$\frac{\lambda(t_i)}{T_i} = \frac{\lambda(t_f)}{T_f}. \quad (9)$$

Moreover, $\dot{\lambda}(t)$ should satisfy the same constraint as Eq. (5) such that $H = H_o$ at the initial and final time. We do not need to care about the system's temperature within the evolution. According to the Liouville theorem, the distribution function is invariant along the phase-space trajectory. Then the ensemble-averaged trajectory entropy is also invariant since the trajectory entropy is proportional to the natural logarithm of the distribution function [29]. Hence, the evolution is along an adiabatic path without exchange of heat or variation of entropy.

We notice that in recent Refs. [52,53], “adiabatic” refers to “very slow,” and “shortcuts to adiabaticity” contain all finite-time schemes producing the desired evolutions which can be achieved naturally in the quasistatic processes. In this paper, however, “shortcut to adiabaticity” corresponds to the thermodynamic adiabatic process in the Carnot cycle which means no exchange of heat and no variation of entropy. Similarly, “shortcut to isothermality” corresponds to the quasistatic isothermal process in the Carnot cycle where the effective temperature of the system is a constant.

III. MODEL AND ENERGETICS

We construct a microscopic engine with a one-dimensional Brownian particle in a time-dependent harmonic potential. This engine contains two isothermal and two adiabatic

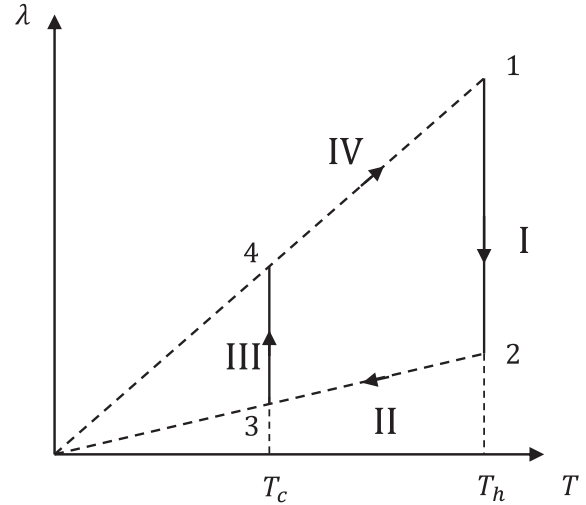


FIG. 1. Carnot-like thermodynamic cycle.

branches which are realized by shortcuts to isothermality and shortcuts to adiabaticity, respectively. The original potential is $U_o = \lambda^2(t)x^2/2$. U_a and H_c are respectively applied to the particle during the isothermal and the adiabatic branches. Figure 1 is a schematic diagram of the thermodynamic cycle. Stage I ranging from time t_1 to t_2 represents the isothermal expansion branch where the particle is coupled to the hot bath with temperature T_h and λ decreases with time. Stage II from time t_2 to t_3 represents the adiabatic expansion branch where the particle is decoupled from the heat bath. Stage III from time t_3 to t_4 represents the isothermal compression branch where the particle is coupled to the cold bath with temperature $T_c (< T_h)$ and λ increases with time. Stage IV represents the adiabatic compression branch after which the particle is again coupled to the hot bath.

Stage I is realized by shortcuts to isothermality. According to Eq. (6), the input work during this stage is expressed as

$$W_I = T_h \ln \frac{\lambda_2}{\lambda_1} + T_h \frac{C_h[\Lambda_h]}{t_2 - t_1}, \quad (10)$$

where

$$C_h[\Lambda_h] = \int_0^1 d\tilde{t} \left(\frac{1}{\gamma_h} + \frac{\gamma_h}{\Lambda_h^2} \right) \frac{1}{\Lambda_h^2} \left(\frac{d\Lambda_h}{d\tilde{t}} \right)^2, \quad (11)$$

and $\Lambda_h = \Lambda_h(\tilde{t}) = \lambda[(t_2 - t_1)\tilde{t} + t_1]$. γ_h is the damping coefficient of the particle in the hot bath. λ_1 and λ_2 are respectively the values of λ at the initial and the final time of stage I. Since the initial and final states of this stage are equilibrium states with the same temperature T_h , we obtain that the energy difference between them vanishes. Based on the conservation of energy, the heat absorbed from the hot bath is

$$Q_I = -W_I = T_h \ln \frac{\lambda_1}{\lambda_2} - T_h \frac{C_h[\Lambda_h]}{t_2 - t_1}. \quad (12)$$

Similarly, the heat exchange between the particle and the cold bath during stage III may be expressed as

$$Q_{III} = T_c \ln \frac{\lambda_3}{\lambda_4} - T_c \frac{C_c[\Lambda_c]}{t_4 - t_3}, \quad (13)$$

where

$$C_c[\Lambda_c] = \int_0^1 d\tilde{t} \left(\frac{1}{\gamma_c} + \frac{\gamma_c}{\Lambda_c^2} \right) \frac{1}{\Lambda_c^2} \left(\frac{d\Lambda_c}{d\tilde{t}} \right)^2, \quad (14)$$

and $\Lambda_c = \Lambda_c(\tilde{t}) = \lambda[(t_4 - t_3)\tilde{t} + t_3]$. γ_c is the damping coefficient of the particle in the cold bath. λ_3 and λ_4 are respectively the values of λ at the initial and final time of stage III.

It should be emphasized that $\ln(\lambda_1/\lambda_2)$ in Eq. (12) and $\ln(\lambda_3/\lambda_4)$ in Eq. (13) are exactly the variations of entropy of the Brownian particle (working substance) during the isothermal expansion and compression branches, respectively. Considering that stages II and IV are realized by shortcuts to adiabaticity, we have $\lambda_2/T_h = \lambda_3/T_c$ and $\lambda_4/T_c = \lambda_1/T_h$ according to Eq. (9). Hence,

$$\frac{\lambda_1}{\lambda_2} = \frac{\lambda_4}{\lambda_3}, \quad (15)$$

which implies that the variations of entropy of the Brownian particle in the two isothermal branches are opposite numbers. Then Eqs. (12) and (13) can be further expressed as

$$Q_I = T_h \left(\Delta S - \frac{C_h}{\tau_h} \right), \quad (16)$$

and

$$Q_{III} = T_c \left(-\Delta S - \frac{C_c}{\tau_c} \right), \quad (17)$$

where $\Delta S = \ln(\lambda_1/\lambda_2) = -\ln(\lambda_3/\lambda_4)$ represents the variation of entropy of the Brownian particle during the isothermal expansion branch. C_h and C_c are respectively the values of the functionals in Eqs. (11) and (14). We have set $\tau_h = t_2 - t_1$ and $\tau_c = t_4 - t_3$ for convenience. Noticing that the dissipative terms [i.e., the second terms in the parentheses in Eqs. (16) and (17)] are inversely proportional to the operation time, we conclude that the microscopic engine based on shortcuts to isothermality and shortcuts to adiabaticity is a realization of microscopic low-dissipation heat engines [8]. C_h and C_c respectively correspond to the dissipation coefficients during the isothermal expansion and compression branches in Ref. [8].

Since the particle will return to the initial state after finishing a thermodynamic cycle, the variation of energy in the cycle vanishes. And there is no heat exchange in the adiabatic branches. Hence, the total output work in each cycle is

$$W_{\text{out}} = Q_I + Q_{III}, \quad (18)$$

with the consideration of energy conservation.

IV. EFFICIENCY AT MAXIMUM POWER

Considering that shortcuts to adiabaticity can be completed rapidly enough [29,41] so that the adiabatic duration is much shorter than the isothermal duration, the total time for completing the cycle can be approximated by $(\tau_h + \tau_c)$. Thus, the power output of this microscopic engine is

$$P = \frac{W_{\text{out}}}{\tau_h + \tau_c} = \frac{T_h(\Delta S - \frac{C_h}{\tau_h}) - T_c(\Delta S + \frac{C_c}{\tau_c})}{\tau_h + \tau_c}. \quad (19)$$

The power output (19) can be optimized with respect to both the protocol of external parameter $\lambda(t)$ and the time τ_h and τ_c .

First, following the thoughts in Ref. [5], to obtain the maximum work output, we need to minimize the functionals $C_h[\Lambda_h]$ and $C_c[\Lambda_c]$ with fixed $\Lambda_h(0)$, $\Lambda_h(1)$, $\Lambda_c(0)$ and $\Lambda_c(1)$. The integrands in Eqs. (11) and (14) can be seen as ‘‘Lagrangians,’’ i.e., $\mathcal{L}_{h,c} = (\frac{1}{\gamma_{h,c}} + \frac{\gamma_{h,c}}{\Lambda_{h,c}^2}) \frac{\Lambda_{h,c}^2}{\Lambda_{h,c}^2}$ with $\Lambda'_{h,c} = d\Lambda_{h,c}/d\tilde{t}$. Since these ‘‘Lagrangians’’ do not explicitly contain the argument of ‘‘time’’ \tilde{t} , the corresponding ‘‘energy functions’’ ($\Lambda'_{h,c} \frac{\partial \mathcal{L}_{h,c}}{\partial \Lambda'_{h,c}} - \mathcal{L}_{h,c}$) are conserved quantities that are respectively expressed as

$$\Sigma_h = \left(\frac{1}{\gamma_h} + \frac{\gamma_h}{\Lambda_h^2} \right) \frac{1}{\Lambda_h^2} \left(\frac{d\Lambda_h}{d\tilde{t}} \right)^2, \quad (20)$$

$$\Sigma_c = \left(\frac{1}{\gamma_c} + \frac{\gamma_c}{\Lambda_c^2} \right) \frac{1}{\Lambda_c^2} \left(\frac{d\Lambda_c}{d\tilde{t}} \right)^2. \quad (21)$$

Noticing that $\Sigma_h = \mathcal{L}_h$ and $\Sigma_c = \mathcal{L}_c$, the minimum values of functionals in Eqs. (11) and (14) are equal to Σ_h and Σ_c , respectively. The optimal protocols $\Lambda_h^*(\tilde{t})$ and $\Lambda_c^*(\tilde{t})$ in isothermal branches are determined by the differential Eqs. (20) and (21) with given values of $\Lambda_h(0)$, $\Lambda_h(1)$, $\Lambda_c(0)$, and $\Lambda_c(1)$. Detailed calculations can be found in Appendix A. In adiabatic branches, there is arbitrariness in selecting the protocols. For example, in Ref. [29] the author chose $\lambda(t) = \lambda_i + (\lambda_f - \lambda_i)\Phi[(t - t_i)/(t_f - t_i)]$, where $\Phi(t)$ is defined as $\Phi(t) = 3t^2 - 2t^3$.

Second, by solving $\partial P/\partial \tau_h = 0$ and $\partial P/\partial \tau_c = 0$, we obtain the optimum values of τ_h and τ_c :

$$\tau_h^* = \frac{2(\sqrt{\Sigma_h \Sigma_c T_h T_c} + \Sigma_h T_h)}{(T_h - T_c)\Delta S}, \quad (22)$$

$$\tau_c^* = \frac{2(\sqrt{\Sigma_h \Sigma_c T_h T_c} + \Sigma_c T_c)}{(T_h - T_c)\Delta S},$$

where we have replaced C_h and C_c with their optimal values Σ_h and Σ_c , respectively. Substituting Eq. (22) into the expression of power, then we obtain the maximum power

$$P_{\text{max}} = \frac{T_h \Delta S^2}{\Sigma_h} \frac{\eta_C^2}{4(\sqrt{(1 - \eta_C)\chi} + 1)^2}, \quad (23)$$

where $\eta_C = 1 - T_c/T_h$ and $\chi = \Sigma_c/\Sigma_h$. Based on the definition of efficiency $\eta = W_{\text{out}}/Q_I$, we derive the efficiency at maximum power:

$$\eta_{P_{\text{max}}} = \frac{\eta_C}{2 - \frac{\eta_C}{\sqrt{\chi(1 - \eta_C)} + 1}}. \quad (24)$$

It is not hard to verify that $\eta_C/2 \leq \eta_{P_{\text{max}}} \leq \eta_C/(2 - \eta_C)$. This constraint is consistent with the conclusion in Ref. [8]. Different from the abstract model in Ref. [8], here we can obtain the exact expressions of Σ_h and Σ_c according to differential Eqs. (20) and (21):

$$\Sigma_h = \frac{1}{\gamma_h} \left[\psi \left(\frac{\lambda_2}{\gamma_h} \right) - \psi \left(\frac{\lambda_1}{\gamma_h} \right) \right]^2, \quad (25)$$

$$\Sigma_c = \frac{1}{\gamma_c} \left[\psi \left(\frac{\lambda_4}{\gamma_c} \right) - \psi \left(\frac{\lambda_3}{\gamma_c} \right) \right]^2, \quad (26)$$

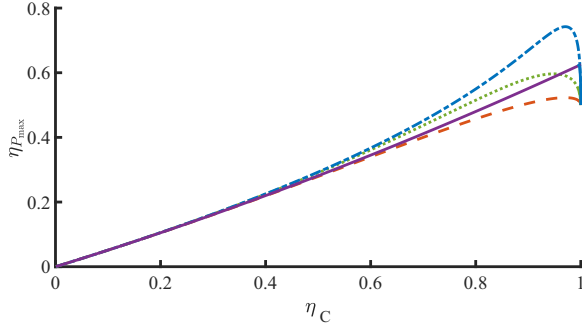


FIG. 2. Efficiency at maximum power with $\xi = 1$ and $\zeta = 0.3$. The dashed, dotted, and dash-dotted lines respectively correspond to Eq. (24) with $\alpha = \pi/10$, $\alpha = 2\pi$, and $\alpha = 10\pi$. The solid line corresponds to Eq. (1) up to the quadratic term.

with $\psi(x) = \sinh^{-1}(x) - \cosh[\sinh^{-1}(1/x)]$. Detailed derivation can be found in Appendix A. Then we have

$$\chi = \frac{\Sigma_c}{\Sigma_h} = \xi \frac{\Psi((1 - \eta_C)\xi\alpha)}{\Psi(\alpha)}, \quad (27)$$

where $\xi \equiv \gamma_h/\gamma_c$, $\alpha \equiv \lambda_1/\gamma_h$ and $\Psi(x) \equiv [\psi(\zeta x) - \psi(x)]^2$ with $\zeta \equiv \lambda_2/\lambda_1$.

The efficiency at maximum power depends on the parameters α , ζ , and ξ as well as the Carnot efficiency η_C . For symmetric damping situation where $\xi = 1$, Eq. (27) becomes $\chi \approx 1 - [\alpha\Psi'(\alpha)/\Psi(\alpha)]\eta_C$ for small η_C . By substituting χ into Eq. (24), we verify that the efficiency at maximum power is consistent with the universal law (1) up to the quadratic term. The underlying reason for this engine coinciding with the universal law up to the quadratic term is that it satisfies the tight coupling and symmetric coupling conditions [10–13]. Specifically, There is no heat leakage between the two baths, and the first term of the Taylor series of χ at $\eta_C = 0$ is 1. The damping coefficients are usually dependent on temperature, which causes ξ deviating from 1. However, we find that $\xi = 1 + O(\eta_C)$ for most solvents [54–56]. In this case, the expansion result of $\eta_{P_{max}}$ still coincides with Eq. (1). In Fig. 2, we compare the behavior of Eq. (1) with that of Eq. (24) for different α when $\xi = 1$ and $\zeta = 0.3$. The dashed, dotted and dash-dotted lines respectively correspond to Eq. (24) with $\alpha = \pi/10$, $\alpha = 2\pi$, and $\alpha = 10\pi$. The solid line corresponds to the universal law (1) up to the quadratic term. We observe that these curves overlap at small η_C .

Moreover, we notice that the efficiency at maximum power (24) tends to be 1/2 when η_C tends to be 1. This surprising result is different from the performances of the endoreversible Carnot-like engine [3,4], the stochastic engine [5], Feynman's ratchet [6], the quantum dot engine [7], etc., while similar behavior has appeared in Ref. [37] for a large-dissipation stochastic engine realized by fast-forward approach. To understand this result, we calculate the Laurent series of χ about $\eta_C = 1$ when $\xi = 1$:

$$\chi|_{\eta_C \rightarrow 1} = \frac{(1 - \zeta)^2}{\zeta^2 \alpha^2 \Psi(\alpha)(1 - \eta_C)^2} + O[(1 - \eta_C)^0]. \quad (28)$$

Substituting this equation into Eq. (24), then we obtain

$$\eta_{P_{max}}|_{\eta_C \rightarrow 1} = \frac{1}{2} + \frac{\zeta \alpha \sqrt{\Psi(\alpha)}}{4(1 - \zeta)} \sqrt{1 - \eta_C} + O[(1 - \eta_C)^1]. \quad (29)$$

The above equation describes the behavior of the three curves corresponding to Eq. (24) nearby $\eta_C = 1$ in Fig. 2. The first item is identical to that in Ref. [37] while the second item is different.

Furthermore, we investigate the efficiency at maximum power in the highly underdamped limit that is $\alpha \gg 1$. Considering that $\psi(x)$ can be expressed as $-\sqrt{1 + 1/x^2} + \ln(x + \sqrt{1 + x^2})$, $\Psi(x)$ tends to $(\ln \zeta)^2$ when $x \gg 1$. Hence, χ tends to 1 under the conditions of $\xi = 1$ and $\alpha \gg 1$ as long as $\eta_C \neq 1$. Substituting $\chi = 1$ into Eq. (24), we find that $\eta_{P_{max}}$ equals the efficiency at maximum power of endoreversible engines [3,4],

$$\eta_{P_{max}}^{\text{under}} = 1 - \sqrt{1 - \eta_C}. \quad (30)$$

The recoveries of endoreversible engines in weak damping cases were previously found in Refs. [22,36,37].

Finally, in the overdamped limit where $\alpha \ll 1$,

$$\Psi[(1 - \eta_C)\xi\alpha] \sim \frac{(1 - \zeta)^2}{\xi^2 \zeta^2 (1 - \eta_C)^2 \alpha^2}, \quad (31a)$$

$$\Psi(\alpha) \sim \frac{(1 - \zeta)^2}{\zeta^2 \alpha^2}. \quad (31b)$$

Substituting the above expressions into Eq. (27), we obtain that $\chi = 1/(1 - \eta_C)^2$ when $\xi = 1$. Now the efficiency at maximum power becomes

$$\begin{aligned} \eta_{P_{max}}^{\text{over}} &= \frac{\eta_C}{2 - \frac{\eta_C \sqrt{1 - \eta_C}}{1 + \sqrt{1 - \eta_C}}} \\ &\approx \frac{1}{2} \eta_C + \frac{1}{8} \eta_C^2 + 0 - \frac{3}{128} \eta_C^4 \quad (\text{small } \eta_C). \end{aligned} \quad (32)$$

Compared with the efficiencies at maximum power of overdamped microscopic engines in previous references [5,34], the result (32) is slightly less than those in Refs. [5,34] starting from the cubic term. The underlying reason for this difference is that shortcuts to isothermality make the values of the dissipation coefficients confined.

V. MAXIMUM POWER AT ANY GIVEN EFFICIENCY

Since the efficiency and power could not be simultaneously optimized, we need to investigate the trade-off relation between these two quantities. For asymmetrical damping coefficients and anharmonic potentials, the microscopic model in the present work becomes a general microscopic low-dissipation engine. In this section, we start with general low-dissipation engines and find the maximum power at given efficiency.

To simplify the calculations, we define the following quantities: $\alpha_h = \Sigma_h/\Delta S$, $\alpha_c = \Sigma_c/\Delta S$, $L_h = \alpha_h/\tau_h$, $L_c = \alpha_c/\tau_c$, $\tilde{\tau} = \tau_h/\tau_c$. The expressions of heat exchanges Q_I and Q_{III} with the new variables are respectively

$$Q_I = \Delta S T_h (1 - L_h), \quad (33)$$

and

$$Q_{\text{III}} = -\Delta S T_c (1 + L_c). \quad (34)$$

Hence, the efficiency of the engine is

$$\eta = \frac{Q_1 + Q_{\text{III}}}{Q_1} = 1 - (1 - \eta_C) \frac{1 + \chi \tilde{\tau} L_h}{1 - L_h}, \quad (35)$$

where we have used $L_c/L_h = \chi \tilde{\tau}$. From Eq. (35), we obtain

$$\tilde{\tau} = b \left(\frac{\delta}{L_h} - 1 \right), \quad (36)$$

where

$$b = \frac{1 - \eta}{(1 - \eta_C)\chi}, \quad (37)$$

and

$$\delta = \frac{\eta_C - \eta}{1 - \eta} \leq \eta_C. \quad (38)$$

Since $\tilde{\tau} \geq 0$ and $b \geq 0$, we obtain $L_h \leq \delta \leq \eta_C$. The power of the engine is

$$P = \frac{\eta Q_1}{\tau_h + \tau_c} = \eta \Delta S \frac{T_h L_h (1 - L_h) (\delta - L_h)}{\alpha_h \delta - L_h + L_h/b}. \quad (39)$$

In the following, we consider the dimensionless power

$$\tilde{P} = \frac{\alpha_h P}{T_h \Delta S} = \eta \frac{L_h (1 - L_h) (\delta - L_h)}{\delta - L_h + L_h/b}. \quad (40)$$

To obtain the maximum value of \tilde{P} for given η , we need to solve the equation $\partial \tilde{P} / \partial L_h = 0$ for L_h . However, this is a cubic equation and the solutions are so cumbersome that we can not illustrate their analytical behavior. Hence, we consider three limiting cases as follows.

First, $\chi \equiv \Sigma_c / \Sigma_h \rightarrow 0$, which means the dissipation is dominated by the isothermal expansion branch. In this case, Eq. (37) implies $b \rightarrow \infty$. Hence, Eq. (40) degenerates into

$$\tilde{P}_0 = \eta L_h (1 - L_h). \quad (41)$$

For given efficiency, this is a parabolic function of L_h with the extreme point at $L_h = 1/2$. Since $L_h \leq \delta \leq \eta_C$, the accessible maximum value of \tilde{P}_0 is dependent on δ . If $\delta \geq 1/2$, which means $\eta \leq 2\eta_C - 1$, then \tilde{P}_0 reaches its maximum value at $L_h = 1/2$ and the value is

$$\tilde{P}_0^* = \frac{\eta}{4}. \quad (42)$$

If $\delta < 1/2$, which means $\eta > 2\eta_C - 1$, then \tilde{P}_0 reaches its maximum value at $L_h = \delta$ and the value is

$$\tilde{P}_0^* = \frac{\eta(1 - \eta_C)(\eta_C - \eta)}{(1 - \eta)^2}. \quad (43)$$

The global maximum value of \tilde{P}_0^* is $\eta_C^2/4$ at $\eta = \eta_C/(2 - \eta_C)$. We emphasize that the value of η_C determines whether the maximum power at given efficiency can be expressed as Eq. (42). If $\eta_C \leq 1/2$, then Eq. (38) implies $\delta \leq 1/2$ for $\eta \in [0, \eta_C]$. Then the maximum power at given efficiency is only expressed as Eq. (43). If $\eta_C > 1/2$, then Eq. (38) implies that δ can be either larger or smaller than $1/2$. Then the maximum power at given efficiency is piecewisely expressed as Eqs. (42) and (43). Figure 3 shows the maximum power

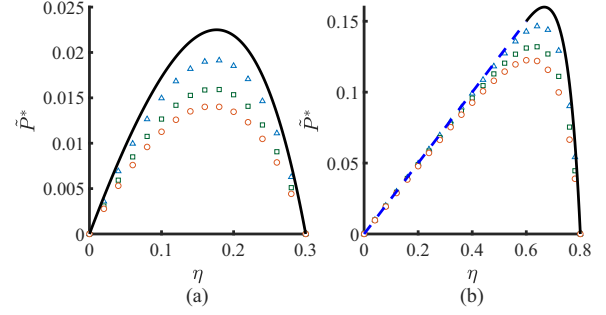


FIG. 3. The maximum power at given efficiency for small χ . The dashed and solid lines correspond to Eqs. (42) and (43), respectively. The triangles, squares, and circles respectively represent the maximum values of power for $\chi = 0.01$, $\chi = 0.05$, and $\chi = 0.1$, which are obtained by numerical method. (a) $\eta_C = 0.3$; (b) $\eta_C = 0.8$.

at given efficiency for small χ when $\eta_C = 0.3$ [Fig. 3(a)] and $\eta_C = 0.8$ [Fig. 3(b)]. The dashed and solid lines correspond to the analytical results (42) and (43), respectively. The triangles, squares, and circles respectively represent the maximum values of power for $\chi = 0.01$, $\chi = 0.05$, and $\chi = 0.1$, which are obtained with numerical method (see Appendix B). From Fig. 3, we observe that the numerical results approach the analytical result as χ decreases.

Second, $\chi = 1$ which implies that the dissipation coefficients are symmetric in the two isothermal branches. In this case, Eq. (37) implies $b = (1 - \eta)/(1 - \eta_C)$. Hence, Eq. (40) degenerates into

$$\tilde{P}_1 = \eta L_h (\delta - L_h) / \delta. \quad (44)$$

Obviously, for given efficiency, \tilde{P}_1 reaches its maximum value at $L_h = \delta/2$. The maximum value is

$$\tilde{P}_1^* = \frac{\eta(\eta_C - \eta)}{4(1 - \eta)}. \quad (45)$$

This expression is the same as the result of endoreversible engine obtained by Chen and Yan [4]. Abiuso and Perarnau-Llobet also obtained such constraint on power for symmetric low-dissipation engines [25]. The global maximum value of \tilde{P}_1^* is $(1 - \sqrt{1 - \eta_C})^2/4$ at $\eta = 1 - \sqrt{1 - \eta_C}$ which is exactly the efficiency at maximum power obtained by Curzon and Ahlborn [3]. Figure 4 shows the maximum power (45) at given efficiency for $\chi = 1$.

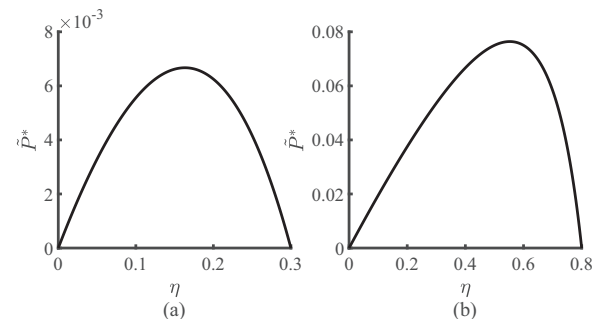


FIG. 4. The maximum power at given efficiency for $\chi = 1$ according to Eq. (45). (a) $\eta_C = 0.3$; (b) $\eta_C = 0.8$.

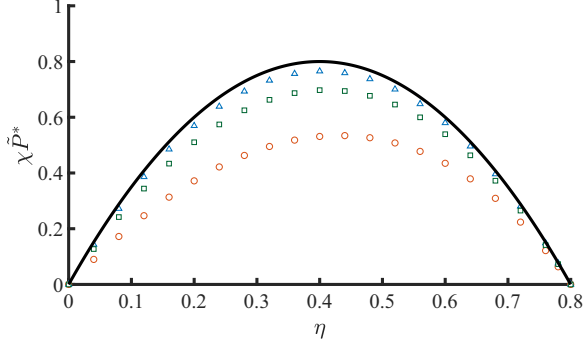


FIG. 5. The product of χ and the maximum power at given efficiency for large χ . The solid line corresponds to the analytical result based on Eq. (47). The circles, squares and triangles respectively correspond to the numerical results for $\chi = 10^2$, $\chi = 10^3$, and $\chi = 10^4$. $\eta_C = 0.8$.

Third, $\chi \rightarrow \infty$ which means the dissipation is dominated by the isothermal compression branch. In this case, Eq. (37) implies $b \rightarrow 0$. The leading term of Eq. (40) is

$$\tilde{P}_\infty = \frac{1}{\chi_\infty} \frac{\eta(1-\eta)}{1-\eta_C} (1-L_h)(\delta-L_h), \quad (46)$$

where the subscript “ ∞ ” of χ_∞ indicates that χ is sufficiently large. For given efficiency, the maximum value of \tilde{P}_∞ is attained when $L_h = 0$ and the maximum value is

$$\tilde{P}_\infty^* = \frac{1}{\chi_\infty} \frac{\eta(\eta_C - \eta)}{1 - \eta_C}. \quad (47)$$

The global maximum value of \tilde{P}_∞^* is $\eta_C^2/[4\chi_\infty(1-\eta_C)]$ at $\eta = \eta_C/2$. Figure 5 shows the behavior of $\chi\tilde{P}^*$ for large χ . The solid line corresponds to the analytical result based on Eq. (47). The circles, squares and triangles respectively correspond to the numerical results for $\chi = 10^2$, $\chi = 10^3$, and $\chi = 10^4$ (the numerical method can be found in Appendix B). From Fig. 5, we observe that the numerical results approach the analytical result as χ increases.

VI. BOUNDS OF EFFICIENCY AT ANY GIVEN POWER

In Sec. V, we have investigated the maximum power at given efficiency and obtained the maximum-power curves in the power-versus-efficiency diagram. In fact, the maximum power at given efficiency and the bounds of efficiency at given power are described by the same expression (detailed mathematical proof can be found in Appendix C) and this expression is the optimal relation between power and efficiency. Hence, the maximum-power curves in Sec. V also provide the upper and lower bounds of efficiency at given power which were studied in Refs. [19,24]. Holubec and Ryabov discussed the upper and lower limits of maximum efficiency at given power in Ref. [19] while Ma *et al.* analyzed the maximum and minimum possible efficiencies at given power in Ref. [24]. In this section, we compare the optimal relations between power and efficiency obtained in Sec. V with those in Refs. [19,24].

The power of the engine can be expressed with $\tilde{\tau}$ and L_h as follows:

$$\begin{aligned} P &= \frac{Q_I + Q_{III}}{\tau_h + \tau_c} \\ &= \frac{\Delta ST_h}{\alpha_h} \tilde{\tau} L_h \frac{(1-L_h) - (1-\eta_C)(1+\chi\tilde{\tau}L_h)}{1+\tilde{\tau}}, \end{aligned} \quad (48)$$

while the efficiency is expressed as Eq. (35). To ensure that the power and the operation time are nonnegative, the value of L_h is confined by $0 \leq L_h \leq \eta_C$ and $\tilde{\tau}$ is confined by $0 \leq \tilde{\tau} \leq [(1-L_h)/(1-\eta_C) - 1]/(\chi L_h)$. Figure 6 shows the efficiency-versus-power diagram of the low-dissipation engines in three limiting cases: $\chi \rightarrow 0$, 1, and ∞ . The scatter points represent the possible values of power and efficiency, which are generated by random values of L_h and $\tilde{\tau}$ according to Eqs. (35) and (48).

Figure 6(a) shows the results for $\chi \rightarrow 0$. The solid line is depicted according to Eqs. (42) and (43). It is exactly the envelope curve of all scatter points. The two dotted lines represent the maximum and minimum possible efficiencies at given power obtained in Ref. [24]. The maximum possible efficiency in Ref. [24] overlaps with our result while the minimum one is inaccessible. Furthermore, the upper bound of efficiency offered by the solid line in this case (i.e., $\chi \rightarrow 0$) is consistent with the upper limit of maximum efficiency at given power obtained in Ref. [19] which is not shown here. Figure 6(b) shows the results for $\chi = 1$. The solid line is depicted according to Eq. (45). It is the envelope curve of all scatter points. The two dotted lines still represent the results in Ref. [24]. The maximum possible efficiency is tight for most power values while the minimum possible efficiency is still inaccessible. The two dashed lines represent the lower and upper limits of maximum efficiency in Ref. [19]. It is obvious that the upper bound offered by the solid line in this case (i.e., $\chi = 1$) is between the two limits in Ref. [19]. Figure 6(c) shows the results for $\chi \rightarrow \infty$. The solid line as an envelope curve of the scatter points, is depicted according to Eq. (47) and it overlaps with the constraints in Ref. [24]. Furthermore, the upper bound of efficiency offered by the solid line in this case (i.e., $\chi \rightarrow \infty$) is consistent with the lower limit of maximum efficiency at given power in Ref. [19]. Based on the above discussion, we conclude that the results in Sec. V provide more exactly optimal relation between power and efficiency than the constraints in Ref. [19,24] at given χ for low-dissipation engines.

VII. CONCLUSION

In summary, we have designed a Carnot-like microscopic heat engine with the help of shortcuts to isothermality and shortcuts to adiabaticity. The dissipative work during the isothermal branches is inversely proportional to the operation time, which means we have realized a microscopic low-dissipation engine. Although we have only demonstrated the case of harmonic potential, this realization is not restricted to harmonic potential since the inverse-proportion relation is independent of the form of potentials according to the character of shortcuts to isothermality as long as these potentials are well-behaved. We have obtained the analytical efficiency at maximum power of this engine with explicit expressions

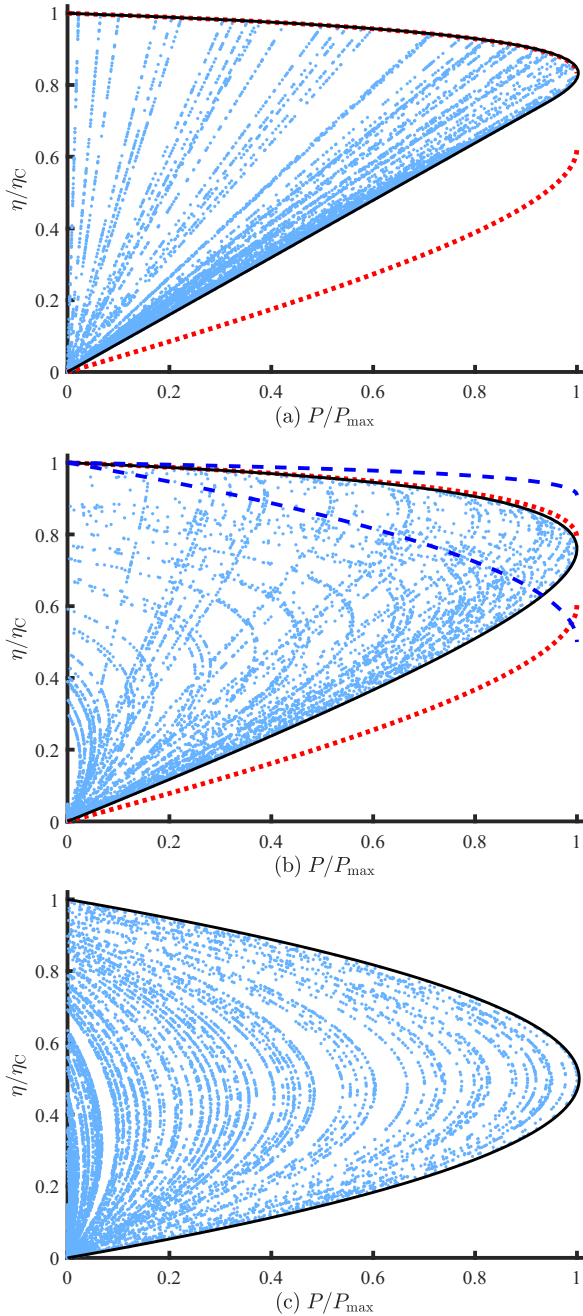


FIG. 6. The efficiency-versus-power diagram of low-dissipation engines. $\eta_C = 0.8$ and P_{\max} is given by Eq. (23). The scatter points are generated by random values of L_h and $\tilde{\tau}$. The solid lines are based on the results in Sec. V. The dashed and dotted lines respectively correspond to the results in Refs. [19] and [24]. (a) $\chi = 10^{-5}$, (b) $\chi = 1$, (c) $\chi = 10^6$.

of dissipation coefficients under the optimized protocols. For symmetric damping coefficients, we have verified that the efficiency at maximum power satisfies the universal law up to the quadratic term (1) at small η_C and tends to a specific value (i.e., $1/2$) when η_C approaches one. In highly underdamped case, the efficiency at maximum power of endoreversible engines is recovered when $\eta_C \neq 1$. Our results are different from those obtained by Schmiedl and Seifert [5]. The underlying

reason is the consideration of shortcuts to isothermality and shortcuts to adiabaticity in our model.

For asymmetrical damping coefficients and anharmonic potentials, the microscopic model in the present work becomes a general microscopic low-dissipation engine. We have investigated the maximum power at given efficiency for general low-dissipation engines and derived the analytical results in three limiting cases. When the ratio χ of the dissipation coefficients during the cold isothermal branch and the hot isothermal branch is one, the result for endoreversible engine is recovered. For χ approaches zero or infinity, the expression of maximum power at given efficiency becomes fairly concise, which is respectively piecewise curve or parabolic curve. In the two limiting cases, the maximum powers agree with the results for the optimized thermodynamic cycles with two finite-sized reservoirs [57] by replacing the efficiency at maximum work in the latter with the Carnot efficiency. Furthermore, because these results provide the optimal relations between power and efficiency, we have compared the bounds of efficiency at given power in the present work with those in Refs. [19,24] and discovered that our bounds are more exact for given χ . Since Albay *et al.* have experimentally realized the shortcuts to isothermality [58–60], it is possible to verify our theoretical results in future experiments. Considering that it may be difficult to decouple the Brownian particle from the heat bath so that the adiabatic processes can be performed, we conceive the idea of imitating the viscous friction force and random thermal force in the real bath by an external field. Similar realizations which raise the effective temperature of Brownian particles can be found in Refs. [33,61]. We notice that in recent works, Abiuso *et al.* optimized the low-dissipation engines via considering the geometric lower bound on entropy production [25,62]. In addition, Chen implemented the strategies of generalized shortcuts to isothermality to design Brownian heat engines and obtained the efficiency at maximum power as well as the maximum power at given efficiency via thermodynamic length [63]. It is worth considering to refine our model in the framework of thermodynamic geometry in the future work.

ACKNOWLEDGMENTS

The authors are very grateful for the discussion with G. Li and Y.-H. Ma. We are grateful for financial support from the National Natural Science Foundation of China (Grant No. 11975050).

APPENDIX A: DETAILED DISCUSSION ABOUT OPTIMAL POTENTIAL PROTOCOLS

Based on the differential Eqs. (20) and (21), the optimal protocols $[\Lambda_h^*(\tilde{t})$ and $\Lambda_c^*(\tilde{t})$] of external parameters are given by the following implicit expressions:

$$\sinh^{-1}\left(\frac{\Lambda_h^*(\tilde{t})}{\gamma_h}\right) - \cosh\left[\sinh^{-1}\left(\frac{\gamma_h}{\Lambda_h^*(\tilde{t})}\right)\right] = -\sqrt{\gamma_h \Sigma_h \tilde{t}} + c_1, \quad (\text{A1})$$

$$\sinh^{-1}\left(\frac{\Lambda_c^*(\tilde{t})}{\gamma_c}\right) - \cosh\left[\sinh^{-1}\left(\frac{\gamma_c}{\Lambda_c^*(\tilde{t})}\right)\right] = \sqrt{\gamma_c \Sigma_c \tilde{t}} + c_2, \quad (\text{A2})$$

where Σ_h , c_1 , Σ_c , and c_2 are time-independent constants which can be determined by the boundary conditions $\Lambda_h(0) = \lambda_1$, $\Lambda_h(1) = \lambda_2$, $\Lambda_c(0) = \lambda_3$, and $\Lambda_c(1) = \lambda_4$. The expressions of these constants are

$$c_1 = \psi\left(\frac{\lambda_1}{\gamma_h}\right), \Sigma_h = \frac{1}{\gamma_h} \left[\psi\left(\frac{\lambda_2}{\gamma_h}\right) - \psi\left(\frac{\lambda_1}{\gamma_h}\right) \right]^2, \quad (\text{A3})$$

$$c_2 = \psi\left(\frac{\lambda_3}{\gamma_c}\right), \Sigma_c = \frac{1}{\gamma_c} \left[\psi\left(\frac{\lambda_4}{\gamma_c}\right) - \psi\left(\frac{\lambda_3}{\gamma_c}\right) \right]^2. \quad (\text{A4})$$

ψ is defined as $\psi(x) \equiv \sinh^{-1}(x) - \cosh[\sinh^{-1}(1/x)]$.

However, considering that $d\Lambda_h(\tilde{t})/d\tilde{t} = \tau_h d\lambda(t)/dt$, the constraint (5) means that

$$\left. \frac{d\Lambda_h(\tilde{t})}{d\tilde{t}} \right|_{\tilde{t}=0} = \left. \frac{d\Lambda_h(\tilde{t})}{d\tilde{t}} \right|_{\tilde{t}=1} = 0. \quad (\text{A5})$$

If we substitute the above conditions into Eq. (20), then we will obtain $\Sigma_h = 0$ (considering that Σ_h is a conserved quantity during the optimal isothermal expansion branch). This is incompatible with Eq. (A3) since $\lambda_1 \neq \lambda_2$. There is same contradiction in the isothermal compression branch.

To resolve these contradictions, it is required that $d\Lambda_{h,c}(\tilde{t})/d\tilde{t}$ jumps from a vanishing (nonvanishing) value to a nonvanishing (vanishing) value at $\tilde{t} = 0$ ($\tilde{t} = 1$), while $\Lambda_{h,c}(\tilde{t})$ is always continuous. The discontinuity of $d\Lambda_{h,c}(\tilde{t})/d\tilde{t}$ makes the calculation of ensemble-averaged work in isothermal branches slightly different from that in the continuous-derivative case. However, we are going to verify that there is no difference in the results of the ensemble-averaged work. Taking the isothermal expansion branch as an example, considering that $d\Lambda_h(\tilde{t})/d\tilde{t}$ is discontinuous and so is $\lambda_h(t)$ where $\lambda_h(t) = \Lambda_h[(t-t_1)/(t_2-t_1)]$, we divide the ensemble-averaged work into three parts in chronological order: instantaneous work W_1^a from $t = t_1^-$ to $t = t_1^+$, continuous work W_1^b from $t = t_1^+$ to $t = t_2^-$, and another instantaneous work W_1^c from $t = t_2^-$ to $t = t_2^+$. The duration of W_1^a and W_1^c is so short that the distribution function does not change and there is no heat exchange between the system and the hot bath. Hence, W_1^a and W_1^c respectively equal to the jump of energy at $t = t_1$ and $t = t_2$. Considering that $\lambda_h(t_1^-) = 0$ and $\lambda_h(t_1^+) = \lambda_h(t_1^+) = \lambda_1$,

$$\begin{aligned} W_1^a &= \langle H_o(x, p, t) + U_a(x, p, t) \rangle_{t_1^-}^{t_1^+} \\ &= \langle U_a(x, p, t) \rangle_{t_1^+}, \end{aligned} \quad (\text{A6})$$

where $f(x)|_a^b = f(b) - f(a)$ and $f(x)|_a = f(a)$. Similarly, considering that $\lambda_h(t_2^+) = 0$ and $\lambda_h(t_2^-) = \lambda_h(t_2^-) = \lambda_2$,

$$W_1^c = -\langle U_a(x, p, t) \rangle_{t_2^-}. \quad (\text{A7})$$

The ensemble-averaged work from $t = t_1^+$ to $t = t_2^-$ follows the definition of trajectory works:

$$\begin{aligned} W_1^b &= \left\langle \int_{t_1^+}^{t_2^-} dt \left(\frac{\partial H_o}{\partial \lambda_h} \dot{\lambda}_h + \frac{\partial U_a}{\partial \lambda_h} \dot{\lambda}_h + \frac{\partial U_a}{\partial \dot{\lambda}_h} \ddot{\lambda}_h \right) \right\rangle \\ &= \int_{t_1^+}^{t_2^-} dt \left\langle \left(\frac{\partial H_o}{\partial \lambda_h} \dot{\lambda}_h + \frac{\partial U_a}{\partial \lambda_h} \dot{\lambda}_h \right) \right\rangle + \dot{\lambda}_h \left\langle \frac{\partial U_a}{\partial \dot{\lambda}_h} \right\rangle_{t_1^+}^{t_2^-} \end{aligned}$$

$$\begin{aligned} &- \int_{t_1^+}^{t_2^-} dt \dot{\lambda}_h \frac{d}{dt} \left\langle \frac{\partial U_a}{\partial \dot{\lambda}_h} \right\rangle \\ &= \int_{t_1^+}^{t_2^-} dt \left[\left\langle \left(\frac{\partial H_o}{\partial \lambda_h} \dot{\lambda}_h + \frac{\partial U_a}{\partial \lambda_h} \dot{\lambda}_h \right) \right\rangle - \dot{\lambda}_h \frac{d}{dt} \left\langle \frac{\partial U_a}{\partial \dot{\lambda}_h} \right\rangle \right] \\ &+ \langle U_a(x, p, t) \rangle_{t_1^+}^{t_2^-}. \end{aligned} \quad (\text{A8})$$

Here we have used the fact that $U_a(x, p, t)$ can be decomposed as $\dot{\lambda}_h f(x, p, \lambda_h)$. The total work during the isothermal expansion branch with discontinuous $\dot{\lambda}_h(t)$ at the endpoints is

$$\begin{aligned} W_1 &= W_1^a + W_1^b + W_1^c \\ &= \int_{t_1^+}^{t_2^-} dt \left[\left\langle \left(\frac{\partial H_o}{\partial \lambda_h} \dot{\lambda}_h + \frac{\partial U_a}{\partial \lambda_h} \dot{\lambda}_h \right) \right\rangle - \dot{\lambda}_h \frac{d}{dt} \left\langle \frac{\partial U_a}{\partial \dot{\lambda}_h} \right\rangle \right]. \end{aligned} \quad (\text{A9})$$

However, if the protocol $\lambda_h(t)$ and its time-derivative $\dot{\lambda}_h(t)$ are all continuous, where $\lambda_h(t_1) = \lambda_1$, $\lambda_h(t_2) = \lambda_2$ and $\dot{\lambda}_h(t_1) = \dot{\lambda}_h(t_2) = 0$, then the ensemble-averaged work from $t = t_1$ to $t = t_2$ is

$$\begin{aligned} W_1 &= \left\langle \int_{t_1}^{t_2} dt \left(\frac{\partial H_o}{\partial \lambda_h} \dot{\lambda}_h + \frac{\partial U_a}{\partial \lambda_h} \dot{\lambda}_h + \frac{\partial U_a}{\partial \dot{\lambda}_h} \ddot{\lambda}_h \right) \right\rangle \\ &= \int_{t_1}^{t_2} dt \left[\left\langle \left(\frac{\partial H_o}{\partial \lambda_h} \dot{\lambda}_h + \frac{\partial U_a}{\partial \lambda_h} \dot{\lambda}_h \right) \right\rangle - \dot{\lambda}_h \frac{d}{dt} \left\langle \frac{\partial U_a}{\partial \dot{\lambda}_h} \right\rangle \right]. \end{aligned} \quad (\text{A10})$$

The result of Eq. (A10) is in the same form as that of Eq. (A9).

Substituting $H_o = p^2/2 + \lambda_h^{*2} x^2/2$ and $U_a = \frac{\dot{\lambda}_h^*}{2\gamma_h \lambda_h^*} [(p - \gamma_h x)^2 + \lambda_h^{*2} x^2]$ where $\lambda_h^*(t) = \Lambda_h^*[(t-t_1)/(t_2-t_1)]$ into Eq. (A9), we obtain

$$W_1 = T_h \ln \frac{\lambda_2}{\lambda_1} + \frac{T_h}{t_2 - t_1} \Sigma_h. \quad (\text{A11})$$

Hence, the optimal protocols in isothermal branches are determined by Eqs. (A1)–(A4) while the time derivatives of the protocols jump from vanishing (nonvanishing) values to nonvanishing (vanishing) values at the initial (final) time of the branches. The finite jumps in the time-derivatives of the protocols at the two ends do not influence the expressions of dissipation coefficients. It is worth noting that discontinuities in the optimal protocols can also be found in Refs. [64,65].

APPENDIX B: NUMERICAL METHOD OF DETERMINING THE MAXIMUM POWER AT GIVEN EFFICIENCY

To find the maximum power at given efficiency, we need to solve the equation $\partial \tilde{P} / \partial L_h = 0$ for L_h . According to Eq. (40), the equation turns out to be

$$(1 + \delta - 2L_h)L_h^2 + b(\delta - L_h)^2(-1 + 2L_h) = 0, \quad (\text{B1})$$

where $b = (1 - \eta)/[(1 - \eta_C)\chi]$ and $\delta = (\eta_C - \eta)/(1 - \eta)$. This is a cubic equation. It has three roots and what we need is the real roots L_h^* that satisfy $0 \leq L_h^* \leq \delta$. The analytical solutions are so cumbersome that it is hard to determine the proper solutions. Hence, we numerically solve Eq. (B1) at certain efficiency with given η_C and χ and pick out the proper solutions L_h^* . Then we compare the value of \tilde{P} at $L_h = L_h^*$ with the boundary values (\tilde{P} at $L_h = 0, \delta$) and obtain the maximum value of power at certain efficiency with given η_C and χ .

APPENDIX C: MATHEMATICAL PROOF OF THE IDENTITY BETWEEN THE MAXIMUM POWER AT GIVEN EFFICIENCY AND THE BOUNDS OF EFFICIENCY AT GIVEN POWER

The relation between \tilde{P} , η , and L_h is expressed as Eq. (40) which can be rewritten as follows:

$$f(\tilde{P}, \eta, L_h) = \eta \frac{L_h(1-L_h)[(\eta_C - \eta) - L_h(1-\eta)]}{(\eta_C - \eta) - L_h(1-\eta) + L_h(1-\eta_C)\chi} - \tilde{P} \equiv 0. \quad (\text{C1})$$

For given η^s , the derivative of $f(\tilde{P}, \eta^s, L_h)$ with respect to L_h is

$$\frac{df(\tilde{P}, \eta^s, L_h)}{dL_h} = \left[\frac{\partial f(\tilde{P}, \eta^s, L_h)}{\partial \tilde{P}} \right]_{L_h} \frac{\partial \tilde{P}}{\partial L_h} + \left[\frac{\partial f(\tilde{P}, \eta^s, L_h)}{\partial L_h} \right]_{\tilde{P}} = 0, \quad (\text{C2})$$

where $[\dots]_{\mathbf{x}}$ means performing the partial derivatives at fixed \mathbf{x} . The optimal L_h that makes \tilde{P} approach its extremal value is obtained by solving the equation $\partial \tilde{P} / \partial L_h = 0$, that is

$$\frac{\partial \tilde{P}}{\partial L_h} = - \frac{[\partial f(\tilde{P}, \eta^s, L_h) / \partial L_h]_{\tilde{P}}}{[\partial f(\tilde{P}, \eta^s, L_h) / \partial \tilde{P}]_{L_h}} = 0. \quad (\text{C3})$$

However, for given \tilde{P}^s , the derivative of $f(\tilde{P}^s, \eta, L_h)$ with respect to L_h is

$$\frac{df(\tilde{P}^s, \eta, L_h)}{dL_h} = \left[\frac{\partial f(\tilde{P}^s, \eta, L_h)}{\partial \eta} \right]_{L_h} \frac{\partial \eta}{\partial L_h} + \left[\frac{\partial f(\tilde{P}^s, \eta, L_h)}{\partial L_h} \right]_{\eta} = 0. \quad (\text{C4})$$

The optimal L_h that makes η approach its extremal value is obtained by solving the equation $\partial \eta / \partial L_h = 0$, that is

$$\frac{\partial \eta}{\partial L_h} = - \frac{[\partial f(\tilde{P}^s, \eta, L_h) / \partial L_h]_{\eta}}{[\partial f(\tilde{P}^s, \eta, L_h) / \partial \eta]_{L_h}} = 0. \quad (\text{C5})$$

Comparing Eqs. (C3) and (C5), we find that the optimal L_h for maximizing both \tilde{P} and η is determined by the same equation,

$$\left[\frac{\partial f(\tilde{P}, \eta, L_h)}{\partial L_h} \right]_{\tilde{P}, \eta} = 0, \quad (\text{C6})$$

as long as $[\partial f(\tilde{P}, \eta, L_h) / \partial \tilde{P}]_{L_h, \eta}$ and $[\partial f(\tilde{P}, \eta, L_h) / \partial \eta]_{L_h, \tilde{P}}$ are not divergent. Substituting the optimal L_h into Eq. (C1), then we obtain the optimal relation between power and efficiency. Divergence of $[\partial f(\tilde{P}, \eta, L_h) / \partial \tilde{P}]_{L_h, \eta}$ or $[\partial f(\tilde{P}, \eta, L_h) / \partial \eta]_{L_h, \tilde{P}}$ may happen at isolated points but it will not influence the ultimate shape of the optimal curve between power and efficiency.

In the limit of $\chi \rightarrow 0$ or $\chi \rightarrow \infty$, however, the optimal relations between power and efficiency may not be determined by the solutions of Eq. (C6) but are determined by the boundary values of L_h . For example, according to the analysis in Sec. V, the maximum power at given efficiency in the limit of $\chi \rightarrow \infty$ is achieved at $L_h = 0$. It can be verified as follows that in this limit the bounds of efficiency at given power are also achieved at $L_h = 0$. Deriving from Eq. (C1), we obtain

that the efficiencies at given power are the solutions of

$$(1-L_h)^2 \eta^2 - \left[(1-L_h)(\eta_C - L_h) + \tilde{P} \left(\frac{1}{L_h} - 1 \right) \right] \eta + \left[\left(\frac{\eta_C}{L_h} - 1 \right) \tilde{P} + (1-\eta_C)\chi \tilde{P} \right] = 0. \quad (\text{C7})$$

In the limit of $\chi \rightarrow \infty$, Eq. (46) implies that \tilde{P} is rather small and $\tilde{P}\chi$ is a normal number. Hence, the above equation can be simplified as follows

$$(1-L_h)^2 \eta^2 - (1-L_h)(\eta_C - L_h)\eta + (1-\eta_C)\chi_\infty \tilde{P} = 0. \quad (\text{C8})$$

To ensure that the solutions of Eq. (C8) are real and positive, there are constraints on L_h :

$$0 \leq L_h \leq \eta_C - 2\sqrt{(1-\eta_C)\chi_\infty \tilde{P}}. \quad (\text{C9})$$

The first inequality is due to the condition that the duration of isothermal branches is positive. The second inequality is due to the condition that the discriminant of Eq. (C8) is nonnegative as well as $L_h \leq \eta_C$. Then we work out the efficiency at given power:

$$\eta_{\pm} = \frac{(\eta_C - L_h) \pm \sqrt{\wp}}{2(1-L_h)}, \quad (\text{C10})$$

where $\wp = (\eta_C - L_h)^2 - 4(1-\eta_C)\chi_\infty \tilde{P}$. The upper bound of efficiencies with different L_h is determined by the maximum value of η_+ and the lower bound of efficiencies is determined by the minimum value of η_- . Since

$$\frac{\partial \eta_+}{\partial L_h} = \frac{(1-\eta_C)[L_h - \eta_C - 4\tilde{P}\chi_\infty - \sqrt{\wp}]}{2(1-L_h)^2 \sqrt{\wp}}, \quad (\text{C11})$$

and $L_h \leq \eta_C \leq 1$, η_+ decreases monotonically from $L_h = 0$ to $L_h = \eta_C - 2\sqrt{(1-\eta_C)\chi_\infty \tilde{P}}$. Hence, the maximum value of η_+ is achieved at $L_h = 0$ and the maximum value is

$$\eta_+^* = \frac{\eta_C}{2} + \frac{1}{2}\sqrt{\eta_C^2 - 4\tilde{P}\chi_\infty(1-\eta_C)}. \quad (\text{C12})$$

Similarly, it can be verified that η_- increases monotonically from $L_h = 0$ to $L_h = \eta_C - 2\sqrt{(1-\eta_C)\chi_\infty \tilde{P}}$. Hence, the minimum value of η_- is also achieved at $L_h = 0$ and the minimum value is

$$\eta_-^* = \frac{\eta_C}{2} - \frac{1}{2}\sqrt{\eta_C^2 - 4\tilde{P}\chi_\infty(1-\eta_C)}. \quad (\text{C13})$$

The relations (C12) and (C13) are consistent with Eq. (47). Another limiting case where $\chi \rightarrow 0$ can be analyzed in the same way.

In a word, the maximum power at given efficiency and the bounds of efficiency at given power are described by the same expression whatever χ is. In fact, as shown in Fig. 6, the scatter points which represent the possible values of efficiency and power of low-dissipation engines at certain χ are encased by a continuous curve. In the present coordinates, this curve provides the bounds of efficiency at given power. If we rotate the diagram 90 degrees counterclockwise, then the curve will become the maximum power at given efficiency.

- [1] L. Chen and F. Sun (eds.), *Advances in Finite Time Thermodynamics: Analysis and Optimization* (Nova Science Publishing, Hauppauge, NY, 2004).
- [2] A. Bejan, *Advanced Engineering Thermodynamics*, 4th ed. (Wiley, Hoboken, NJ, 2016).
- [3] F. L. Curzon and B. Ahlborn, Efficiency of a Carnot engine at maximum power output, *Am. J. Phys.* **43**, 22 (1975).
- [4] L. Chen and Z. Yan, The effect of heat-transfer law on performance of a two-heat-source endoreversible cycle, *J. Chem. Phys.* **90**, 3740 (1989).
- [5] T. Schmiedl and U. Seifert, Efficiency at maximum power: An analytically solvable model for stochastic heat engines, *Europhys. Lett.* **81**, 20003 (2008).
- [6] Z. C. Tu, Efficiency at maximum power of Feynman's ratchet as a heat engine, *J. Phys. A: Math. Theor.* **41**, 312003 (2008).
- [7] M. Esposito, K. Lindenberg, and C. V. den Broeck, Thermoelectric efficiency at maximum power in a quantum dot, *Europhys. Lett.* **85**, 60010 (2009).
- [8] M. Esposito, R. Kawai, K. Lindenberg, and C. Van den Broeck, Efficiency at Maximum Power of Low-Dissipation Carnot Engines, *Phys. Rev. Lett.* **105**, 150603 (2010).
- [9] Y. Izumida and K. Okuda, Efficiency at maximum power of minimally nonlinear irreversible heat engines, *Europhys. Lett.* **97**, 10004 (2012).
- [10] C. Van den Broeck, Thermodynamic Efficiency at Maximum Power, *Phys. Rev. Lett.* **95**, 190602 (2005).
- [11] M. Esposito, K. Lindenberg, and C. Van den Broeck, Universality of Efficiency at Maximum Power, *Phys. Rev. Lett.* **102**, 130602 (2009).
- [12] S. Sheng and Z. C. Tu, Constitutive relation for nonlinear response and universality of efficiency at maximum power for tight-coupling heat engines, *Phys. Rev. E* **91**, 022136 (2015).
- [13] Z.-C. Tu, Abstract models for heat engines, *Front. Phys.* **16**, 33202 (2021).
- [14] J. M. Gordon and M. Huleihil, General performance characteristics of real heat engines, *J. Appl. Phys.* **72**, 829 (1992).
- [15] J. Chen, Z. Yan, G. Lin, and B. Andresen, On the Curzon-Ahlborn efficiency and its connection with the efficiencies of real heat engines, *Energ. Convers. Manag.* **42**, 173 (2001).
- [16] Y. Wang and Z. C. Tu, Bounds of efficiency at maximum power for linear, superlinear and sublinear irreversible Carnot-like heat engines, *Europhys. Lett.* **98**, 40001 (2012).
- [17] W. Yang and T. Zhan-Chun, Bounds of efficiency at maximum power for normal-, sub-, and super-dissipative Carnot-like heat engines, *Commun. Theor. Phys.* **59**, 175 (2013).
- [18] V. Holubec and A. Ryabov, Efficiency at and near maximum power of low-dissipation heat engines, *Phys. Rev. E* **92**, 052125 (2015).
- [19] V. Holubec and A. Ryabov, Maximum efficiency of low-dissipation heat engines at arbitrary power, *J. Stat. Mech.* (2016) 073204.
- [20] A. Ryabov and V. Holubec, Maximum efficiency of steady-state heat engines at arbitrary power, *Phys. Rev. E* **93**, 050101(R) (2016).
- [21] N. Shiraishi, K. Saito, and H. Tasaki, Universal Trade-off Relation Between Power and Efficiency for Heat Engines, *Phys. Rev. Lett.* **117**, 190601 (2016).
- [22] A. Dechant, N. Kiesel, and E. Lutz, Underdamped stochastic heat engine at maximum efficiency, *Europhys. Lett.* **119**, 50003 (2017).
- [23] P. Pietzonka and U. Seifert, Universal Trade-Off Between Power, Efficiency, and Constancy in Steady-State Heat Engines, *Phys. Rev. Lett.* **120**, 190602 (2018).
- [24] Y.-H. Ma, D. Xu, H. Dong, and C.-P. Sun, Universal constraint for efficiency and power of a low-dissipation heat engine, *Phys. Rev. E* **98**, 042112 (2018).
- [25] P. Abiuso and M. Perarnau-Llobet, Optimal Cycles for Low-Dissipation Heat Engines, *Phys. Rev. Lett.* **124**, 110606 (2020).
- [26] J. Wang and J. He, Efficiency at maximum power output of an irreversible Carnot-like cycle with internally dissipative friction, *Phys. Rev. E* **86**, 051112 (2012).
- [27] Y. C. Gerstenmaier, Cyclic heat engines with nonisentropic adiabats and generalization to steady-state devices including thermoelectric converters, *Phys. Rev. E* **105**, 064136 (2022).
- [28] S. Rana, P. S. Pal, A. Saha, and A. M. Jayannavar, Single-particle stochastic heat engine, *Phys. Rev. E* **90**, 042146 (2014).
- [29] Z. C. Tu, Stochastic heat engine with the consideration of inertial effects and shortcuts to adiabaticity, *Phys. Rev. E* **89**, 052148 (2014).
- [30] V. Holubec, An exactly solvable model of a stochastic heat engine: Optimization of power, power fluctuations and efficiency, *J. Stat. Mech.* (2014) P05022.
- [31] V. Blickle and C. Bechinger, Realization of a micrometre-sized stochastic heat engine, *Nat. Phys.* **8**, 143 (2012).
- [32] I. A. Martínez, É. Roldán, L. Dinis, D. Petrov, J. M. R. Parrondo, and R. A. Rica, Brownian Carnot engine, *Nat. Phys.* **12**, 67 (2016).
- [33] I. A. Martínez, É. Roldán, L. Dinis, and R. A. Rica, Colloidal heat engines: A review, *Soft Matter* **13**, 22 (2017).
- [34] C. A. Plata, D. Guéry-Odelin, E. Trizac, and A. Prados, Building an irreversible Carnot-like heat engine with an overdamped harmonic oscillator, *J. Stat. Mech.* (2020) 093207.
- [35] D. S. P. Salazar and S. A. Lira, Stochastic thermodynamics of nonharmonic oscillators in high vacuum, *Phys. Rev. E* **99**, 062119 (2019).
- [36] Y. H. Chen, J.-F. Chen, Z. Fei, and H. T. Quan, Microscopic theory of the Curzon-Ahlborn heat engine based on a Brownian particle, *Phys. Rev. E* **106**, 024105 (2022).
- [37] K. Nakamura, J. Matrasulov, and Y. Izumida, Fastforward approach to stochastic heat engine, *Phys. Rev. E* **102**, 012129 (2020).
- [38] G. Li, H. T. Quan, and Z. C. Tu, Shortcuts to isothermality and nonequilibrium work relations, *Phys. Rev. E* **96**, 012144 (2017).
- [39] G. Li and Z. C. Tu, Equilibrium free-energy differences from a linear nonequilibrium equality, *Phys. Rev. E* **103**, 032146 (2021).
- [40] X. Chen, A. Ruschhaupt, S. Schmidt, A. del Campo, D. Guéry-Odelin, and J. G. Muga, Fast Optimal Frictionless atom Cooling in Harmonic Traps: Shortcut to Adiabaticity, *Phys. Rev. Lett.* **104**, 063002 (2010).
- [41] C. Jarzynski, Generating shortcuts to adiabaticity in quantum and classical dynamics, *Phys. Rev. A* **88**, 040101(R) (2013).
- [42] C. Jarzynski, Nonequilibrium Equality for Free Energy Differences, *Phys. Rev. Lett.* **78**, 2690 (1997).
- [43] K. Sekimoto, *Stochastic Energetics* (Springer, Heidelberg, New York, 2010).
- [44] U. Seifert, Stochastic thermodynamics, fluctuation theorems and molecular machines, *Rep. Prog. Phys.* **75**, 126001 (2012).
- [45] A. Emmanouilidou, X.-G. Zhao, P. Ao, and Q. Niu, Steering an Eigenstate to a Destination, *Phys. Rev. Lett.* **85**, 1626 (2000).

- [46] M. Demirplak and S. A. Rice, Adiabatic population transfer with control fields, *J. Phys. Chem. A* **107**, 9937 (2003).
- [47] M. V. Berry, Transitionless quantum driving, *J. Phys. A: Math. Theor.* **42**, 365303 (2009).
- [48] A. del Campo, Shortcuts to Adiabaticity by Counterdiabatic Driving, *Phys. Rev. Lett.* **111**, 100502 (2013).
- [49] J. Deng, Q.-h. Wang, Z. Liu, P. Hänggi, and J. Gong, Boosting work characteristics and overall heat-engine performance via shortcuts to adiabaticity: Quantum and classical systems, *Phys. Rev. E* **88**, 062122 (2013).
- [50] A. del Campo, J. Goold, and M. Paternostro, More bang for your buck: Super-adiabatic quantum engines, *Sci. Rep.* **4**, 6208 (2014).
- [51] S. Deffner, C. Jarzynski, and A. del Campo, Classical and Quantum Shortcuts to Adiabaticity for Scale-Invariant Driving, *Phys. Rev. X* **4**, 021013 (2014).
- [52] D. Guéry-Odelin, A. Ruschhaupt, A. Kiely, E. Torrontegui, S. Martínez-Garaot, and J. G. Muga, Shortcuts to adiabaticity: Concepts, methods, and applications, *Rev. Mod. Phys.* **91**, 045001 (2019).
- [53] D. Guéry-Odelin, C. Jarzynski, C. A. Plata, A. Prados, and E. Trizac, Driving rapidly while remaining in control: Classical shortcuts from Hamiltonian to stochastic dynamics, [arXiv:2204.11102](https://arxiv.org/abs/2204.11102).
- [54] D. S. Viswanath, T. K. Ghosh, D. H. L. Prasad, N. V. K. Dutt, and K. Y. Rani, *Viscosity of Liquids: Theory, Estimation, Experiment, and Data* (Springer, Dordrecht, 2006).
- [55] R. B. Haj-Kacem, N. Ouerfelli, J. V. Herráez, M. Guettari, H. Hamda, and M. Dallel, Contribution to modeling the viscosity Arrhenius-type equation for some solvents by statistical correlations analysis, *Fluid Phase Equilib.* **383**, 11 (2014).
- [56] A. Messaâdi, N. Dhouibi, H. Hamda, F. B. M. Belgacem, Y. H. Adbelkader, N. Ouerfelli, and A. H. Hamzaoui, A new equation relating the viscosity Arrhenius temperature and the activation energy for some Newtonian classical solvents, *J. Chem.* **2015**, 163262 (2015).
- [57] H. Yuan, Y.-H. Ma, and C. P. Sun, Optimizing thermodynamic cycles with two finite-sized reservoirs, *Phys. Rev. E* **105**, L022101 (2022).
- [58] J. A. C. Albay, S. R. Wulaningrum, C. Kwon, P.-Y. Lai, and Y. Jun, Thermodynamic cost of a shortcuts-toisothermal transport of a Brownian particle, *Phys. Rev. Res.* **1**, 033122 (2019).
- [59] J. A. C. Albay, C. Kwon, P.-Y. Lai, and Y. Jun, Work relation in instantaneous-equilibrium transition of forward and reverse processes, *New J. Phys.* **22**, 123049 (2020).
- [60] J. A. C. Albay, P.-Y. Lai, and Y. Jun, Realization of finite-rate isothermal compression and expansion using optical feedback trap, *Appl. Phys. Lett.* **116**, 103706 (2020).
- [61] I. A. Martínez, É. Roldán, J. M. R. Parrondo, and D. Petrov, Effective heating to several thousand Kelvins of an optically trapped sphere in a liquid, *Phys. Rev. E* **87**, 032159 (2013).
- [62] P. Abiuso, H. J. D. Miller, Martí Perarnau-Llobet and Matteo Scandi, Geometric optimisation of quantum thermodynamic processes, *Entropy* **22**, 1076 (2020).
- [63] J.-F. Chen, Optimizing Brownian heat engine with shortcut strategy, *Phys. Rev. E* **106**, 054108 (2022).
- [64] T. Schmiedl and U. Seifert, Optimal Finite-Time Processes in Stochastic Thermodynamics, *Phys. Rev. Lett.* **98**, 108301 (2007).
- [65] A. Gomez-Marin, T. Schmiedl, and U. Seifert, Optimal protocols for minimal work processes in underdamped stochastic thermodynamics, *J. Chem. Phys.* **129**, 024114 (2008).